4-30-2012

Development and Testing of an Actively Adjustable Stiffness Mechanism

Eleazar Marquez

Robert Freeman

Horacio Vasquez

Proceedings of the ASME 2010 International Mechanical Engineering Congress & Exposition
IMECE2010
November 12-18, 2010, Vancouver, British Columbia, Canada

IMECE2010-39033

Development and Testing of an Actively Adjustable Stiffness Mechanism

Eleazar Marquez
Robert A. Freeman, Ph. D.
Horacio Vasquez, Ph. D.
Department of Mechanical Engineering
The University of Texas – Pan American
1201 W. University Dr.
Edinburg, Texas 78541-2999

ABSTRACT

This study presents the comparison of the theoretical and experimental results of the performance of an adjustable stiffness mechanism. In particular, the use of redundant actuation is emphasized in the design of a one degree-of-freedom Watt II mechanism capable of independently controlling the effective stiffness without a change in equilibrium position. This approach is in contrast to spring mechanism designs unable to actively control the spring rate independent of deflection, and with potential applications in various types of suspension and assembly systems.

Results indicate that two direct drive brush-type direct current motors are required to drive the redundantly actuated mechanism and create a system that behaves as an adjustable stiffness spring.

Keywords: Variable Stiffness, Torque Control, Mechanisms, Dynamics

1. INTRODUCTION

Redundantly actuated mechanical linkage systems contain more force/torque inputs (actuators) than they have kinematic degrees of freedoms. With the implementation of this concept, numerous tasks in assembly and suspension systems can be addressed to enhance their performance. For instance, one task addressed in assembly systems is *load sharing/balancing* (LS/B) among several actuators [7, 8, 9, 10, 11], in which redundant actuation intends to distribute the required operational load in an optimal way to each of the system actuators and, at the same time, maintaining load requirements within an operational range. Several of these applications include Dual Arms (DA), Walking Machines (WM), and manipulators with Direct Drive (DD) substructures. Another application addressed under this category is *disturbance force rejection* (DFR) [15, 16], in which the goal is for one set of actuators to supply the required input loads to achieve the nominal task to be executed, while the redundant inputs are used to counteract disturbance loads. The concept of redundant actuation is also considered in *feedforward impedance control* (FIC) [12, 13, 14]. The purpose of FIC is to work with instabilities encountered in contact tasks such as multi-limbed locomotion and machining and assembly operations. Other applications of redundantly actuated mechanical linkage systems involucrate Serial Arms (SA), Flexible Structures (FS), Magneto and Electro-Static Levitation Systems (LS), Bio-Mechanical Prostheses (BM) and Spring Mechanisms (SM).

Freeman [1] incorporated redundant actuation in the design and control of an active automotive suspension system to achieve a variation in stiffness according to distinct road conditions. Results indicated that five actuators, with one connecting the two suspensions, are required for full stiffness and motion control.

Although the advantage of implementing redundant actuation into several applications has been discussed, no experimental validation exists. In a previous research, a one degree-of-freedom Stephenson III linkage [2] was theoretically modeled and simulated to achieve a desired effective stiffness via redundant actuation, yet it lacked the development and testing of a physical model to validate its performance. Therefore, the purpose of this study is to design, construct, and actively control a one degree-of-freedom, unidirectional, Watt II linkage. Theoretical computations of the nonposition dependent planar mechanism will be validated by developing, implementing, and testing a physical model.

2. MODELING OVERVIEW

A one degree-of-freedom Watt II linkage is designed and redundantly actuated using two direct drive motors to create a system that behaves as an adjustable stiffness spring. In this process, kinematic and kinetic analyses are performed to determine the geometric design of the spring mechanism and estimate its nonlinear behavior. Once these values are computed and validated via Working Model 2D simulation, the physical components of the mechanism were constructed and assembled, and the device was tested for its stiffness variation

capability. In order to drive the redundantly actuated mechanism, brush-type direct current (DC) motors were attached to each of the two grounded revolute joints, and their torque was controlled with corresponding power amplifiers that incorporate current control loops.

In addition, a linear displacement slider is attached to the output end of the system to measure the effective stiffness. Particularly, the effective stiffness of the system depends on the torques (determined based on the desired effective stiffness) generated by the brush-type DC motors, and on the displacement created as a result of an external force. A linear potentiometer and a force sensor was implemented to measure the displacement of the slider. A data acquisition system was additionally employed to measure the motor torques, the slider displacement, and the external disturbance force acting on the slider.

3. DESIGN OF WATT II LINKAGE

The design phase of the active spring mechanism in Figure 1 required a two step process. The first step involved generating the design of the four revolute-four bar (D111) mechanism. In such design, the kinematic and kinetic equations were simulated to determine the equilibrium state of the mechanism and to estimate its non-linear behavior. Once the first step was accomplished, a location was established on Link 4 to design the D011 planar mechanism that completes the desired linkage. In this process, the equilibrium state of the mechanism was determined and its non-linear behavior was estimated as well.

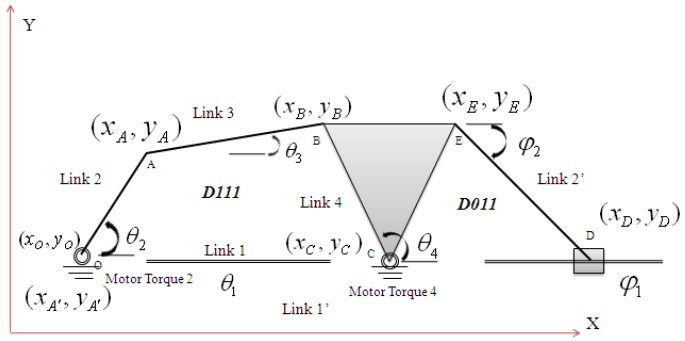

Figure 1: Watt II Linkage

The target in these facets is to describe the motion of the dependent parameters in terms of position, velocity, and acceleration. In this study, the velocity and acceleration are expressed in terms of *g* and *h* function, respectively. These functions are known as the *Kinematic Influence Coefficient* (KIC) and represent the rate of change of the system with respect to time [3-6]. For instance, let the symbol *u* represent any/all dependent parameters and θ_i represent the independent reference/input parameters, applying the chain rule allows to determine the velocity of *u*

$$\frac{d}{dt}u = \left(\frac{d}{d\theta_i}u\right)\cdot\frac{d}{dt}\theta_i \tag{1}$$

where the derivative of *u* with respect to θ_i is referred as the first order KIC, *g*-function, and is defined by

$$g_{ui} = \frac{d}{d\theta_i}u \tag{2}$$

In a similar way, the acceleration of the spring mechanism is obtained by taking the second derivative of *u* with respect to time; from (1):

$$\frac{d^2}{dt^2}u = \left(\frac{d}{d\theta_i}u\right)\cdot\frac{d^2}{dt^2}\theta_i + \left(\frac{d^2}{d\theta_i^2}u\right)\cdot\left(\frac{d}{dt}\theta_i\right)^2 \tag{3}$$

where the *h*-function, known as the second order KIC, is defined as

$$h_{ui} = \frac{d^2}{d\theta_i}u \tag{4}$$

Unsprung Position Analysis D111

The unsprung position analysis of the four revolute-four bar mechanism initiates by specifying several design parameters as illustrated in Table 1. These values are arbitrarily considered by means of fabricating a feasible size physical model.

Table 1: Design Parameters for D111

Units (m)	Units (m)	Units (m)	Units (m)
$X_O = 0$	$X_C = 0.250$	$L_2 = 0.102$	$L_4 = 0.102$
$Y_O = 0$	$Y_C = 0$	$L_3 = 0.153$	$\theta_2 = 45^\circ$

With such parameters defined, the length and relative angle of Link 1 are determined by

$$L_1 = \sqrt{(Y_C - Y_O)^2 + (X_C - X_O)^2} \tag{5}$$

and

$$\theta_1 = \tan^{-1}\left(\frac{Y_C - Y_O}{X_C - X_O}\right) \tag{6}$$

Obtaining the parameters of Link 1 leads to the determination of the coupler angle θ_3 and the output angle θ_4, which are calculated by using the *position loop equations* along the X and Y directions as

$$L_2\cos(\theta_2) + L_3\cos(\theta_3) = L_1\cos(\theta_1) + L_4\cos(\theta_4) \tag{7}$$

and

$$L_2\sin(\theta_2) + L_3\sin(\theta_3) = L_1\sin(\theta_1) + L_4\sin(\theta_4) \tag{8}$$

After manipulating these non-linear equations, two roots are obtained that allow for the unknown parameters to be determined

$$X_a = \frac{-P + \sqrt{P^2 + Q^2 - R^2}}{R - Q} \tag{9}$$

and

$$X_b = \frac{-P - \sqrt{P^2 + Q^2 - R^2}}{R - Q} \tag{10}$$

With these roots, the Tan Half-Angle approach is then implemented to solve for the couple angle θ_3 and the output angle θ_4 as

$$\theta_{3a} = 2\tan^{-1}(X_a) \tag{11}$$

$$\theta_{3b} = 2\tan^{-1}(X_b) \tag{12}$$

$$\theta_{4a} = \tan^{-1}\left(\frac{L_2 S_2 + L_3 S_{3a} - L_1 S_1}{L_2 C_2 + L_3 C_{3a} - L_1 C_1}\right) \tag{13}$$

$$\theta_{4b} = \tan^{-1}\left(\frac{L_2 S_2 + L_3 S_{3b} - L_1 S_1}{L_2 C_2 + L_3 C_{3b} - L_1 C_1}\right) \tag{14}$$

Motion Analysis D111

Attaining the coupler angle and the output angle enables for the determination of the *g* and *h* function of each link with respect to the input of the system. This means that the behavior of the D111 mechanism is analyzed by calculating the angular velocity and acceleration of each link relative to the center of mass, and the translational velocity and acceleration of each link relative to the center of mass as well.

Therefore, expressing the angular velocity of Link 3 and Link 4 relative to the center of mass results in differentiating (7) and (8) with respect to θ_2 in the form of

$$g_{32} = \frac{L_2 \sin(\theta_4 - \theta_2)}{L_3 \sin(\theta_3 - \theta_4)} \tag{15}$$

and

$$g_{42} = \frac{L_2 \sin(\theta_3 - \theta_2)}{L_4 \sin(\theta_3 - \theta_4)} \tag{16}$$

In a similar manner, expressing the angular acceleration of Link 3 and Link 4, relative to the center of mass, is determined by differentiating (15) and (16) with respect to θ_2 as

$$h_{32} = \frac{L_4 {g_{42}}^2 - L_3 {g_{32}}^2 \cos(\theta_4 - \theta_3) - L_2 \cos(\theta_4 - \theta_2)}{L_3 \sin(\theta_4 - \theta_3)} \tag{17}$$

and

$$h_{42} = \frac{L_4 {g_{42}}^2 \cos(\theta_4 - \theta_3) - L_3 {g_{32}}^2 - L_2 \cos(\theta_3 - \theta_2)}{L_4 \sin(\theta_4 - \theta_3)} \tag{18}$$

The motion analysis continues by calculating the *g* and *h* function of each link relative to the center of mass along the X and Y direction of the D111 mechanism. Before continuing, for example, let the location of the center of mass be represented by a local reference frame (*u*,*v*) on the mechanism (Figure 2) as $u_2 = u_3 = u_4 = 1/2$ and $v_2 = v_3 = v_4 = 0$.

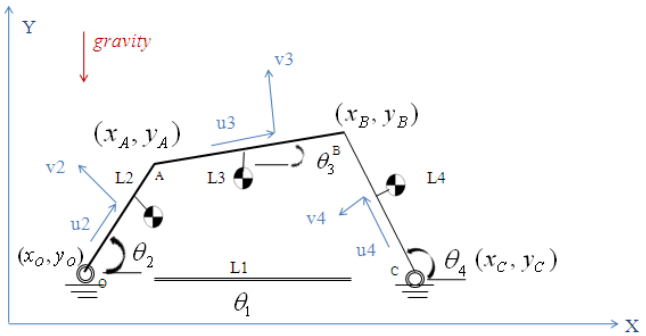

Figure 2: Local Reference Frame

Once the local frame has been established, the KIC's of each link include:

Link 2

$$g_{22x} = -(u_2 \sin(\theta_2) - v_2 \cos(\theta_2)) \tag{19}$$

$$h_{22x} = -(u_2 \cos(\theta_2) - v_2 \sin(\theta_2)) \tag{20}$$

$$g_{22y} = u_2 \cos(\theta_2) + v_2 \sin(\theta_2) \tag{21}$$

$$h_{22y} = -(u_2 \sin(\theta_2) + v_2 \cos(\theta_2)) \tag{22}$$

Link 3

$$g_{32x} = -L_2 \sin(\theta_2) - (u_3 \sin(\theta_3) + v_3 \cos(\theta_3)) \cdot g_{32} \tag{23}$$

$$h_{32x} = -L_2 \cos(\theta_2) - \begin{bmatrix} (u_3 \sin(\theta_3) + v_3 \cos(\theta_3)) \cdot h_{32} \\ + (u_3 \cos(\theta_3) - v_3 \sin(\theta_3)) \cdot g_{32}{}^2 \end{bmatrix} \quad (24)$$

$$g_{32y} = L_2 \cos(\theta_2) + (u_3 \cos(\theta_3) - v_3 \sin(\theta_3)) \cdot g_{32} \quad (25)$$

$$h_{32y} = -L_2 \sin(\theta_2) - \begin{bmatrix} (u_3 \cos(\theta_3) - v_3 \sin(\theta_3)) \cdot h_{32} \\ - (u_3 \sin(\theta_3) + v_3 \cos(\theta_3)) \cdot g_{32}{}^2 \end{bmatrix} \quad (26)$$

Link 4

$$g_{42x} = -(u_4 \sin(\theta_4) + v_4 \cos(\theta_4)) \cdot g_{42} \quad (27)$$

$$h_{42x} = -(u_4 \sin(\theta_4) + v_4 \cos(\theta_4)) \cdot h_{42} - (u_4 \cos(\theta_4) - v_4 \sin(\theta_4)) \cdot g_{42}{}^2 \quad (28)$$

$$g_{42y} = (u_4 \cos(\theta_4) - v_4 \sin(\theta_4)) \cdot g_{42} \quad (29)$$

$$h_{42y} = (u_4 \cos(\theta_4) - v_4 \sin(\theta_4)) \cdot h_{42} - (u_4 \sin(\theta_4) + v_4 \cos(\theta_4)) \cdot g_{42}{}^2 \quad (30)$$

Mass Moment of Inertia

Part of the design process to obtain a system in equilibrium is to determine the mass moment of inertia of each link and the mass moment of inertia of the two grounded revolute joints. Such computations include:

$$I_2 = \frac{1}{12} m_2 L_2{}^2 \quad (31)$$

$$I_3 = \frac{1}{12} m_3 L_3{}^2 \quad (32)$$

$$I_4 = \frac{1}{12} m_4 L_4{}^2 \quad (33)$$

$$I_O = I_2 + m_2 (u_2{}^2 + v_2{}^2) \quad (34)$$

and

$$I_C = I_4 + m_4 (u_4{}^2 + v_4{}^2) \quad (35)$$

Unsprung Position Analysis D011

Similar to the unsprung position analysis of the D111 mechanism, several design parameters are specified for the D011 mechanism (Table 2). Implementing the D011 mechanism as part of the design is accomplished by establishing a new point with respect to Link 4. This process allows for the completion of the design of the Watt II linkage.

Table 2: Design Parameters for D011

$X_{A'} = 0m$	$\theta_{4'} = \theta_4$	$L_{2'} = 0.127m$
$Y_{A'} = 0m$	$\psi_1 = 0^\circ$	$Type = 1$

Therefore, with the specification of these parameters, the unsprung analysis initiates by determining the position of the new point on the mechanism as

$$X_E = X_C + u_E \cos(\theta_4) - v_E \sin(\theta_4) \quad (36)$$

and

$$Y_E = X_C + u_E \sin(\theta_4) + v_E \cos(\theta_4) \quad (37)$$

where $u_E = 0.07m$ and $v_E = -0.080m$. Once the coordinates of the point are generated, the *position loop equations* are implemented to determine the length of the system ($L_{1'}$) and the angle of Link 2' as

$$X_{A'} + L_{1'} \cos(\psi_1) = X_E + L_{2'} \cos(\psi_2) \quad (38)$$

and

$$Y_{A'} + L_{1'} \sin(\psi_1) = Y_E + L_{2'} \sin(\psi_2) \quad (39)$$

where the unknowns are calculated as

$$L_{1'} = (aC_1 + bS_1) + Type \cdot \left[(aC_1 + bS_1)^2 + L_{2'}{}^2 - (a^2 + b^2) \right]^{\frac{1}{2}} \quad (40)$$

and

$$\psi_2 = \tan^{-1} \frac{L_{1'} S_1 - b}{L_{1'} C_1 - a} \quad (41)$$

Motion Analysis of the D011 Mechanism

The motion analysis of the D011 mechanism involves implementing the kinematic and kinetic equations to describe its non-linear behavior relative to the center of mass. For example, the angular velocity of Link 2' is determined by first differentiating the *position loop equations* (38) and (39):

$$g_{L_1'/2} \cos(\psi_1) = g_{E2x} - L_{2'} \sin(\psi_2) \cdot g_{2'2} \quad (42)$$

and

$$g_{L_1'/2}\sin(\psi_1) = g_{E2y} - L_{2'}\cos(\psi_2)\cdot g_{2'2} \tag{43}$$

where the left-hand side of the equations are equivalent to the velocity generated by the output element:

$$g_{D2x} = g_{L_1'/2}\cdot\cos(\psi_1) \tag{44}$$

$$g_{D2y} = g_{L_1'/2}\cdot\sin(\psi_1) \tag{45}$$

Therefore, solving for angular velocity of the link, relative to the center of mass, results in

$$g_{2'2} = \frac{-g_{E2y}}{L_{2'}\cos(\psi_2)} \tag{46}$$

Similarly, the angular acceleration of Link 2' is obtained by differentiating this equation with respect to the input as

$$h_{2'2} = \frac{h_{E2y} - L_{2'}\sin(\psi_2)\cdot {g_{2'2}}^2}{-L_{2'}\cos(\psi_2)} \tag{47}$$

Once the angular velocity and acceleration of Link 2' have been determined, the motion analysis continues by solving for the translational velocity and acceleration of the linear displacement slider (with respect to the center of mass), the link, and the new point E created on the mechanism. Such KICs include the following equations:

Linear Displacement Slider

$$g_{D2x} = g_{E2x} - L_{1'}\sin(\psi_2)\cdot g_{2'2} \tag{48}$$

$$h_{D2x} = h_{E2x} - L_{2'}\cos(\psi_2)\cdot {g_{2'2}}^2 - L_{2'}\sin(\psi_2)\cdot h_{2'2} \tag{49}$$

$$g_{D2y} = 0 \tag{50}$$

$$h_{D2y} = 0 \tag{51}$$

Link 2'

$$g_{2'2x} = -\left(u_{2'}\sin(\psi_2) + v_{2'}\cos(\psi_2)\right)\cdot g_{2'2} \tag{52}$$

$$h_{2'2x} = -\left(u_{2'}\sin(\psi_2) + v_{2'}\cos(\psi_2)\right)\cdot h_{2'2} - \left(u_{2'}\cos(\psi_2) - v_{2'}\sin(\psi_2)\right)\cdot {g_{2'2}}^2 \tag{53}$$

$$g_{2'2y} = \left(u_{2'}\cos(\psi_2) - v_{2'}\sin(\psi_2)\right)\cdot g_{2'2} \tag{54}$$

$$h_{2'2y} = \left(u_{2'}\cos(\psi_2) - v_{2'}\sin(\psi_2)\right)\cdot h_{2'2} - \left(u_{2'}\sin(\psi_2) + v_{2'}\cos(\psi_2)\right)\cdot {g_{2'2}}^2 \tag{55}$$

Point E

$$g_{E2x} = -\left(u_E\cdot\sin(\theta_4) + v_E\cdot\cos(\theta_4)\right)\cdot g_{42} \tag{56}$$

$$h_{E2x} = -\left(u_E\sin(\theta_4) + v_E\cos(\theta_4)\right)\cdot h_{42} - \left(u_E\cos(\theta_4) - v_E\sin(\theta_4)\right)\cdot {g_{42}}^2 \tag{57}$$

$$g_{E2y} = -\left(u_E\cdot\cos(\theta_4) - v_E\cdot\sin(\theta_4)\right)\cdot g_{42} \tag{58}$$

$$h_{E2y} = \left(u_E\cos(\theta_4) - v_E\sin(\theta_4)\right)\cdot h_{42} - \left(u_E\sin(\theta_4) + v_E\cos(\theta_4)\right)\cdot {g_{42}}^2 \tag{59}$$

Motor Torque 2 and Motor Torque 4 via Redundant Actuation

Having determined the geometric design of the Watt II linkage and its non-linear behavior, allows for the calculation of two input forces to be generated. For example, calculating the necessary torque at θ_2 involves equating the model kinetic energy with the system kinetic energy (principle of virtual work). This relationship models the translational kinetic energy with the rotational kinetic energy, which results in the total kinetic energy of the system. Therefore, since the spring is a "planar" mechanism, the kinetic energy of the actual system is written in a general form as

$$K.E._{System} = \sum_l \left(\frac{1}{2}I_l{\dot{\theta}_l}^2 + \frac{1}{2}M_l\left({\dot{x}_l}^2 + {\dot{y}_l}^2\right)\right) \tag{60}$$

where,

l = Links

I_l = Mass moment of inertia of links about the center of mass

$\dot{\theta}_l$ = Absolute angular speed of links

M_l = Mass of links

$\dot{x}_l, \dot{y}_l$ = Absolute velocity components of links with respect to the center of mass

Rearranging this expression, in terms of the KICs, yields the Effective Inertia/Generalized Mass of the system

$$I_{si} = \sum_{1} \left[M_1 \cdot \left[\left(g_{li}{}^{x} \right)^2 + \left(g_{li}{}^{y} \right)^2 \right] + I_1 g_{li}{}^{2} \right] \tag{61}$$

where substituting the respective parameters gives

$$\begin{aligned} I_{2s} &= I_2 \cdot g_{22}{}^{2} + m_2 \cdot \left(g_{22x}{}^{2} + g_{22y}{}^{2} \right) + \\ & I_3 \cdot g_{32}{}^{2} + m_3 \cdot \left(g_{32x}{}^{2} + g_{32y}{}^{2} \right) + \\ & I_4 \cdot g_{42}{}^{2} + m_4 \cdot \left(g_{42x}{}^{2} + g_{42y}{}^{2} \right) + \\ & I_{2'} \cdot g_{2'2}{}^{2} + m_{2'} \cdot \left(g_{2'2x}{}^{2} + g_{2'2y}{}^{2} \right) + I_O + I_C \end{aligned} \tag{62}$$

Furthermore, calculating the input force at θ_2 involves solving for the Effective Stiffness of the system due to Gravity Loads as

$$T_{si} = \sum_{1} - \left[\left(- M_1 \cdot g \right) \cdot g_{li}{}^{y} \right] \tag{63}$$

where g represents the gravitational constant that acts in the negative y-direction, and $g_{li}{}^{y}$ represents the translational velocity of each link along the vertical direction. Therefore, substituting the respective g functions and the respective masses of the links yields

$$\begin{aligned} T_{2s} &= g_{22y} \cdot \left(- m_2 \cdot g \right) + g_{32y} \cdot \left(- m_3 \cdot g \right) \\ &+ g_{42y} \cdot \left(- m_4 \cdot g \right) + g_{2'2y} \cdot \left(- m_{2'} \cdot g \right) \end{aligned} \tag{64}$$

Once the Effective Inertia and the Gravity Loads are computed, the process of finding the equilibrium torques continues by solving for the forces acting on the spring mechanism (Inertial Power). However, before solving for the force, the procedure requires computing the Inertial Load of the system by setting the product between the load and the input velocity equal to the rate of change of the kinetic energy as

$$T_i{}^{I} \dot{\phi}_i = \frac{d}{dt} \left(\frac{1}{2} I_{is} \dot{\phi}_i{}^{2} \right) \tag{65}$$

Solving this general equation requires implementing the chain rule to differentiate with respect to time

$$T_i{}^{I} = I_{is} \ddot{\phi}_i + P_{is} \dot{\phi}_i{}^{2} \tag{66}$$

where P_{is} is the Inertial Power of the system and is expressed as

$$\begin{aligned} P_{si} &= \frac{1}{2} \frac{d}{d\phi_i} I_{si} = \\ & \sum_{1} \left[M_1 \left[\left(g_{li}{}^{x} \cdot h_{li}{}^{x} \right) + \left(g_{li}{}^{y} \cdot h_{li}{}^{y} \right) \right] + I_1 g_{li} h_{li} \right] \end{aligned} \tag{67}$$

Substituting the respective parameters into the equation yields

$$\begin{aligned} P_{2s} &= I_2 \cdot g_{22} \cdot h_{22} + m_2 \cdot \left(g_{22x} h_{22x} + g_{22y} h_{22y} \right) \\ &+ I_3 \cdot g_{32} \cdot h_{32} + \\ & m_3 \cdot \left(g_{32x} h_{32x} + g_{32y} h_{32y} \right) + I_4 \cdot g_{42} \cdot h_{42} \\ &+ m_4 \cdot \left(g_{42x} h_{42x} + g_{42y} h_{42y} \right) + \\ & I_{2'} \cdot g_{2'2} \cdot h_{2'2} + m_{2'} \cdot \left(g_{2'2x} h_{2'2x} + g_{2'2y} h_{2'2y} \right) \end{aligned} \tag{68}$$

Since the objective is to control the effective stiffness about an equilibrium position in the one degree-of-freedom system, at least two actuators, non-collocated and nonlinearly related must exist. Recalling (62), the required motor torque is obtained by adding all the effective loads of the spring mechanism in terms of Newton's second law as

$$\begin{aligned} \sum_{A} \left(T_a g_{ai} \right) = & I_{is} \frac{d^2}{dt^2} \left(\phi_i \right) + P_{is} \left(\frac{d}{dt} \phi_i \right)^2 \\ & - \left(T_{is} \right)^k - \left(T_{is} \right)^g - \left(T_{is} \right)^L - \left(T_i \right)^m \end{aligned} \tag{69}$$

where,

$T_{is}{}^{k}$ = Effective loads

$T_{is}{}^{g}$ = Gravity loads with respect to the center of mass

$T_{is}{}^{L}$ = Externally applied loads

$T_i{}^{m}$ = Motor torque

Therefore, solving for the required motor torque of the spring mechanism at θ_2 involves rearranging the expression to obtain

$$T_{2m} = \left(I_{2s} \cdot \alpha_2 + P_{2s} \cdot \omega_2{}^{2} \right) - \left(T_{2s} \right)^g \tag{70}$$

Lastly, the torque at θ_4 is calculated from the equilibrium equation generated from the concept of virtual work, and is expressed as

$$T_4 = \frac{-T_2}{g_{42}} \tag{71}$$

4. FABRICATION OF THE ACTIVE SPRING MECHANISM

On the manufacturing stage of the spring mechanism, machinability of each component is the first concern that rises before selecting a material. For example, one characteristic that the selected material must have is the feasibility to manufactured under high temperatures and high cutting speeds. Under these conditions, first of all, the material must possess sufficient toughness (ductility) to avoid fracture during plastic deformation. If this characteristic is low, the components might fracture as soon as a small force is applied to the (brittle) surface. This situation, in particular, must be avoided in order to perform smooth and clean cuts. On the other hand, the material should not be too tough that the machines cannot penetrate and create the specified cuts. If the strength of the materials is too high, the manufacturing tools could be damaged or ruined by trying to achieve something beyond their capability. Therefore, the most important factor, to satisfy both of these conditions, is to consider the mechanical properties of the materials, such as the coefficient of thermal expansion, modulus of elasticity, and yield strength. Further considerations consist of selecting a non-corrosive material that conserves the functionality of the system as well as the aesthetics. In this case, a potential corrosion problem occurs because the adjustable spring mechanism is always exposed to the atmosphere and it has lubricant (fluid) applied on the revolute joints and on the output sliding element to minimize friction. *Corrosion* could develop on the metal in a matter of days causing rapid degradation of the system performance. Such phenomena must be avoided in order to have a functional system.

Therefore, after considering such factors, aluminum alloy 6061-T6 was selected as the material needed to fabricate the Watt II linkage. Not only does the aluminum alloy contain the desired mechanical properties, but it is a common material in the marketplace and its cost is relatively low.

By having selected the material, the process of manufacturing the spring mechanism initiated by using the tools and machines needed to fabricate each component according to the design specifications (Figure 3). As mentioned earlier and illustrated on the figure, in order to drive the redundantly actuated mechanism, two direct brush-type DC motors are attached to each of two grounded revolute joints and their torques are controlled with corresponding power amplifiers, which incorporate current control loops. These torques generate internal loading within the system that permit creating an effective stiffness. Therefore, the current and voltage generated by the DC motors are measured and monitored with respective digital multimeters (DMMs).

In addition, two potentiometers are implemented to control the current generated by each motor. One potentiometer functions in a clockwise direction (at θ_2), while the other potentiometer functions in a counterclockwise direction (at θ_4). The output end of the system, on the other hand, is a linear displacement slider which moves along a horizontal frame and its position is measured using a 5-inch linear potentiometer and an additional DMM. The effective stiffness of the system, as referenced to the slider, is dependent on the redundant actuator torques, which are in turn determined based on the desired effective stiffness. Therefore, an external force acting on the slider causes it to go through a displacement that depends on the controllable stiffness of the mechanism. Moreover, the linear potentiometer and a force sensor are used to measure the displacement of the slider and the external force acting on it in order to determine the stiffness of the systems which is adjustable be changing the input torques from the motors.

Figure 3: Watt II Linkage with Control and Monitoring System

5. TESTING AND RESULTS

Before mounting and assembling the variable stiffness mechanism, the relationship between the torque and current of each direct brush-type DC motor was determined. Since the power amplifier utilized in this study has a maximum continuous current of 5A, several current values, in steps of 0.25A, were applied and the static torque that was generated by the motor was measured to attain the required correlation. The initial current applied to the DC motor was 4A and it was progressively decreased to 0.5A. Fans were used to blow room temperature air around the motor to keep them from overheating.

To determine the torque created by each motor, a link was mounted on the shaft and a load cell was positioned at a certain distance to measure the force exerted as the motor intends to rotate. The torque is then calculated by multiplying the force measured by the load cell and the moment arm between the motor axis of rotation and the point of force application.

Figures 4 and 5 illustrate the torque-current relationship generated by each of the brush-type DC motors. As expected, these results indicate that a linearly proportional relationship exists between the generated torque and input current to the DC motor. As a result of this relationship, a series of equilibrium torques (Table 3) were created to measure the effective stiffness of the spring mechanism under each one of those conditions.

Measuring the effective stiffness of the system requires applying different external forces (Table 4) on the slider and measuring its displacement with respect to the horizontal global reference frame. This process is then repeated with a different set of input motor torques to form severalcorrelations that embrace the variation of the mechanism effective stiffness. In particular, three graphs are generated to evaluate the behavior of the actively adjustable spring mechanism: stiffness versus force, stiffness versus displacement, and displacement versus force.

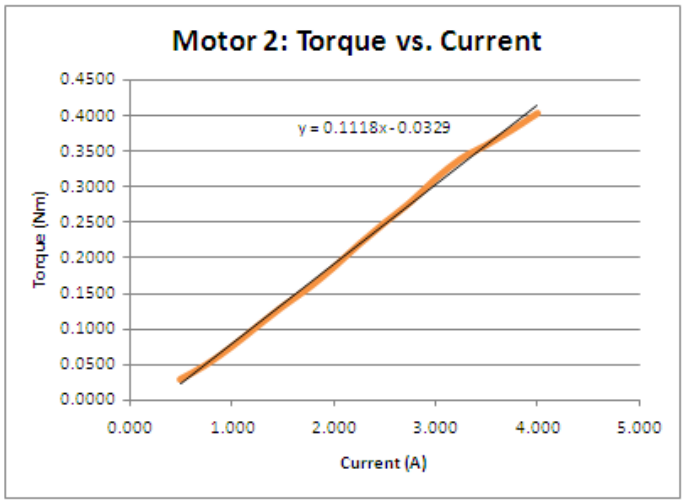

Figure 4: Motor 2 Torque-Current Relationship

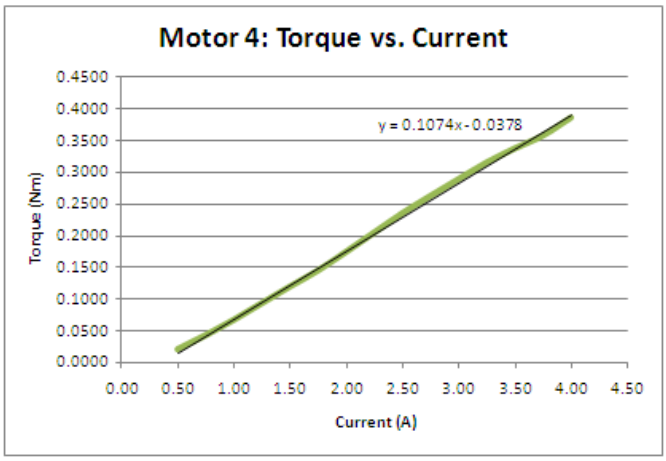

Figure 5: Motor 4 Torque-Current Relationship

Theoretical Results

It is important to mention that the theoretical analyses are based on the development of a frictionless spring mechanism. The fabricated prototype, on the other hand, as any real system, has friction effects as a result of the motor bearings, contact between links and between the slider and its track.. Such friction on the system causes the mechanism to remain motionless as a very small force is applied on the slider. This means that the results generated from testing the physical mechanism may vary slightly with respect to the simulation generated in Working Model 2D. However, in order to avoid more discrepancies between the simulations and the experiments, , the motor parameters are specified on the Working Model simulations. For example, these parameters include the resistance of the motor armature, inductance, speed constant, and torque constant.

The first measurement involves analyzing the effective stiffness of the mechanism as a function of the force applied on the slider (Figure 6). Theoretical results indicate that as the force acting on the slider increases, the effective stiffness decreases as a result of the varying displacement, and thus an inverse proportional relationship is developed. However, as the equilibrium torques (Test 2, Test 3, etc.) increase, the effective stiffness of the linkage increases for the force applied on the slider.

Table 3: Test Plan

Equilibrium Torque				
Test	**C2 (A)**	**T2 (Nm)**	**C4 (A)**	**T4 (Nm)**
1	1.00	-0.07518	1.7290	0.14789
2	1.25	-0.10363	2.1613	0.19432
3	1.50	-0.13208	2.5935	0.24074
4	1.75	-0.15748	3.0258	0.28717
5	2.00	-0.18694	3.4580	0.33359

This means that by applying the same force on the slider and varying the equilibrium torques, the effective stiffness of the system can be adjusted (Figure 7). Therefore, depending on the application or task addressed, different equilibrium torques can be implemented to meet the required system behavior. In addition, the graphical relationship obtained shows the nonlinear behavior of the spring mechanism.

Table 4: Input Forces used in the Experiments

Mass (grams)	**Weight (N)**
50	0.490
70	0.686
100	0.980
120	1.176
150	1.471
170	1.667
200	1.961

Furthermore, the second measurement involves evaluating the displacement of the linear slider as a function of the force applied on it. Five different sets of equilibrium torques were tested. The results in Figure 8 indicate that as the force increases so does the displacement of the slider, denoting that a nonlinear proportional relationship occurs. Nonetheless, implementing higher equilibrium input torques reduce the output displacement and hence the effective stiffness of the mechanism increases.

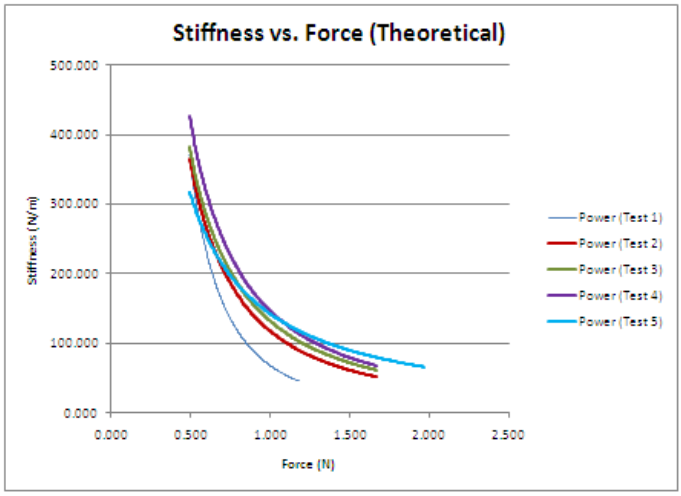

Figure 6: Stiffness as a Function of Force

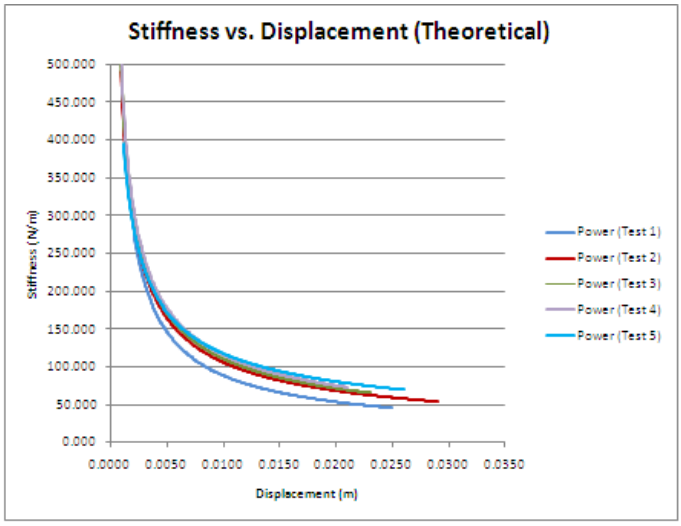

Figure 7: Stiffness as a Function of Displacement

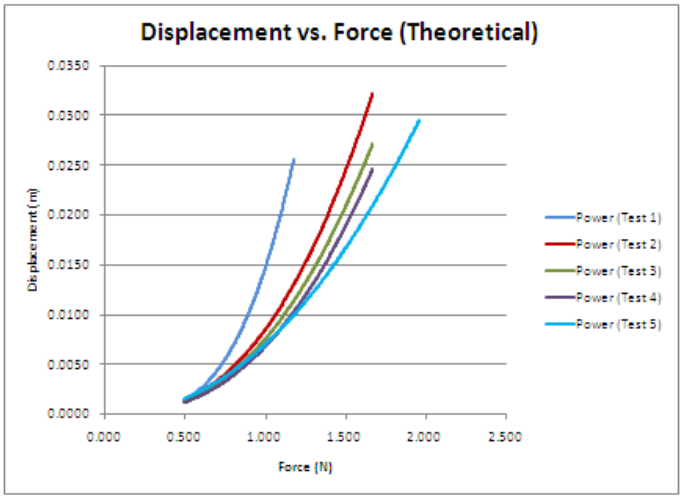

Figure 8: Displacement as a Function of Force

Theoretical versus Experimental Results

The actively adjustable Watt II linkage was constructed and experimentally tested to compare to the theoretical results. Mismatch in the friction effect acting on the system and the model itself produce slightly different results when comparing the simulations and the experiments. In addition, the obtained results indicate that the system behaves as a nonlinear system.

In figures 9 and 10, only the set 1 of equilibrium torques was graphically represented. These results indicate that the experiments and theoretical simulations generate similar results. For instance, the experimental behavior is represented with the dotted lines in Figures 9 and 10, and the theoretical behavior is represented with solid lines. This means that the concept of adjustable springs has proven to be valid and that the mathematical model that was developed closely represents the real system.. Although a slight difference occurs due to the frictional effects, the results are similar.

Moreover, the stiffness as a function of the force was compared in five cases in Figure 11. These results indicate that the relationship between both parameters is an inverse relationship, meaning that as the force increases, the effective stiffness of the mechanism decreases. Therefore, the effective stiffness decreases as the displacement caused by the external force increases (Figure 12). In this case, the theoretical and experimental values are almost identical.

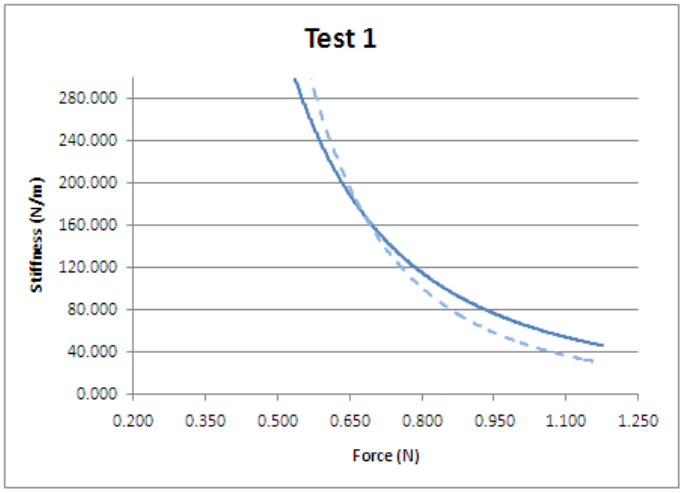

Figure 9: Test 1: Stiffness vs. Force

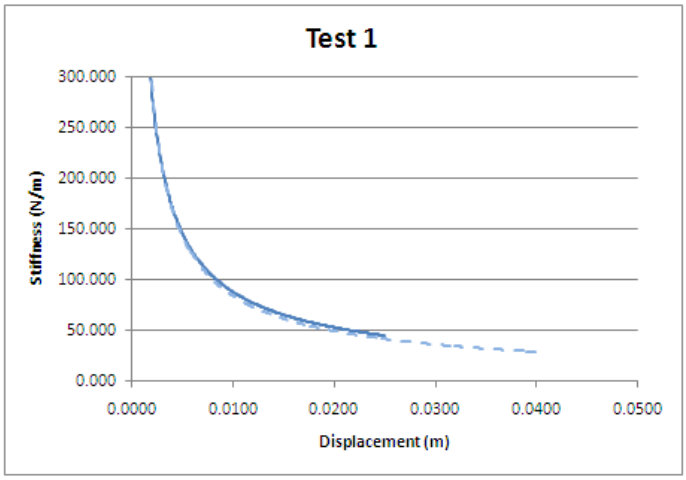

Figure 10: Test 1: Stiffness vs. Displacement

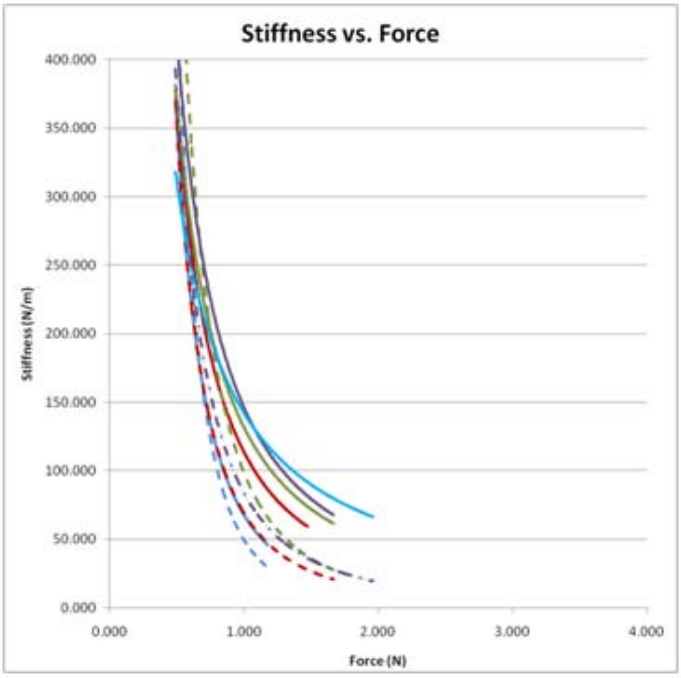

Figure 11: Comparison of Theoretical versus Experimental System Behavior

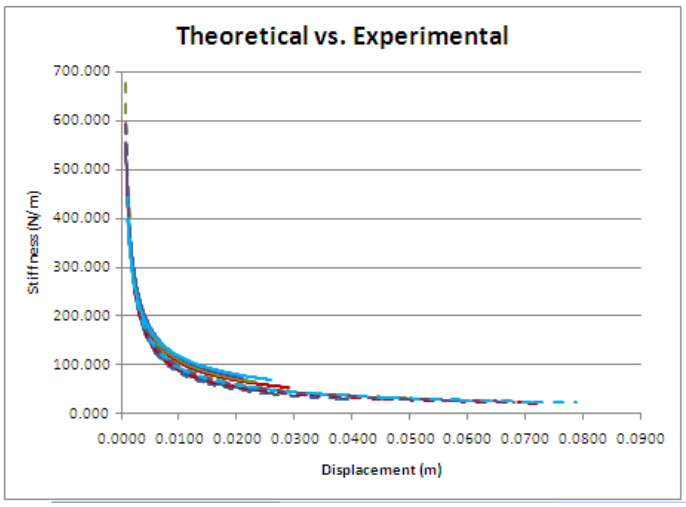

Figure 12: Stiffness as a Function of Displacement

6. CONCLUSIONS

The present study is a comparison of theoretical and experimental results of a variable stiffness mechanism. In particular, a one degree-of-freedom Watt II mechanism was designed and redundantly actuated. From the simulations and the experiments, it can be concluded that the adjustable stiffness system behaves stiffer with small forces and less stiff with high forces. To match the theoretical and the experimental behavior, additional friction effects might have to be taken into account in the simulations. The results indicated that the theoretical and experimental results are similar to each other, meaning that the concept of redundant actuation has been proven to be a way of generating a variable stiffness mechanism.

Future work will consist of additional experimentation and control strategies to simultaneously regulate the stiffness of the system and the position of the slider. The experimental setup developed in this study is also practical enough to perform educational demonstrations of a multidisciplinary system that involves topics in dynamics, controls, and measurements and instrumentation, among others.

REFERENCES

[1] Freeman, R.A., 2004, "Active Suspension Control via Redundant Actuation," Proceedings of the ASME Design Engineering Technical Conference, Vol. 2B, 1043-1054, 2004.

[2] Zhou, L., 1992, "An Actively Adjustable Unidirection Spring Mechanism," Master's thesis, The University of Texas at Austin.

[3] Pollock, S.F., 1975, "Dynamic Model Formulation Programmed for Dyad Based Machines," Master's thesis, The University of Florida.

[4] Freeman, R.A. and Tesar, D., 1982, "The Generalized Coordinate Selection for the Dynamics of Complex Planar Mechanical Systems," Journal of Mechanical Design, **104**, pp.206-217.

[5] Freeman, R.A. and Tesar, D., 1988, "Dynamic Modeling of Serial and Parallel Mechanisms/Robotic Systems: Part – Methodology, Part II- Applications," Proceedings 1988, ASME Mechanisms Conference, DE-Vol. 15-3, 7-27, 1988.

[6] Benedict, C.E. and Tesar D., 1978, Model formulation of complex mechanisms with multiple inputs: Part I-geometry, part II: the dynamic model," Journal of Mechanical Design, **100**, pp. 747-761.

[7] Cheng, F.T. and Orin, D.E. 1989, "Efficient Algorithm for Optimal Force Distribution in Multiple-Chain Robotic Systems- The Compact-Dual LP Algorithm," Proc. IEEE Conf. on Robotics and Automation, Scottsdale, AZ, Vol. 1, pp. 943-950.

[8] Conley, W.J., 1975, "Integration of Nonlinear Springs into Machines by Analytical Synthesis," Master's Thesis, University of Florida, Gainesville.

[9] Hayward, V. and Kurtz, R., 1990. "Modeling a Parallel Wrist Mechanism with Actuator Redundancy," Proc. The 2nd International Workshop on Advanced in Robot Kinematics, Linz Austria.

[10] Kumar, V.J. and Gardner, J., 1990, "Kinematics of Redundantly Actuated Closed Chains," IEEE J. of Robotics and Automation, Vol. 6, No. 2, pp. 269-273.

[11] Roppen, T. and Nakamura, Y., 1990, "Singularity-Free Parameterization and Performance Analysis of Actuation Redundancy," Proc. IEEE Conf. Robotics and Automation, Cincinnati, OH, pp. 806-811.

[12] Cutkosky, M.R. and Wright, P.K., 1986, "Active Control of a Complaint Wrist in Manufacturing Tasks," ASME J. Eng. for Industry, Vol. 108, No.1, pp. 36-43.

[13] Hogan, N., 1982, "Mechanical Impedance Control in Assistive Devices and Manipulators," Robot Motion: Planning and Control, MIT Press, pp. 361-371.

[14] Jacobsen, H.K., Iversen, E.K., and Davis, C.C., 1989, "Antagonistic Control of a Tendon Driven Manipulator," Proc. IEEE Conf. Robotics and Automation, Scottsdale, AZ, Vol. 3, pp. 1334-1339.

[15] West, H.H., 1980, "The Analysis of Structures," McGraw-Hill, New York.

[16] West, H.H., and Asada, H., 1985, “A Method for the Design of Hybrid Position/Force Controllers for Manipulators Constrained by contact with the Environment,” Proc. IEEE Conf. Robotics and Automation, St. Louis, MO, pp. 251-259.